

# Electronic Supplementary Information (ESI) for: Water-Chromophore Electron Transfer Determines the Photochemistry of Cytosine and Cytidine

Rafał Szabla,<sup>\*a,b</sup> Holger Kruse,<sup>b</sup> Jiří Šponer<sup>b</sup> and Robert W. Góra<sup>b</sup>

June 20, 2017

## Video

We attach a short video as supporting material to this article. The video highlights the main conclusions of this work in a pictorial way. In particular, it presents the possible path from the Franck-Condon region towards the minimum on the  $n\pi_{CT}^*$  hypersurface. It also shows the transition from the  $n\pi_{CT}^*$  minimum towards the EDPT conical intersection (see the snapshot in Fig. S1) and the possible reactions which might occur in the electronic ground state afterwards.

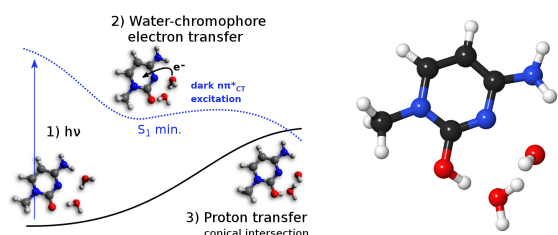


Fig. S1 Snapshot from the attached video presenting the final stage of the EDPT process occurring on the  $n\pi_{CT}^*$  hypersurface.

## Computational Methods

The ground-state equilibrium geometry of the mC-(H<sub>2</sub>O)<sub>2</sub> cluster was optimized at the MP2/cc-pVTZ level,<sup>1</sup> whereas the minimum energy geometries of the S<sub>1</sub> and T<sub>1</sub> states were obtained using the CC2/cc-pVTZ method.<sup>2,3</sup> To verify whether the CC2 method qualitatively reproduces the geometry of the charge transfer excited-state complex with water molecules ( $^1n\pi_{CT}^*$  state), we optimized the S<sub>1</sub> minimum of an analogous cytosine-(H<sub>2</sub>O)<sub>2</sub> cluster using the CASPT2/SA-2-CASSCF(6,5) and the 6-31G\* basis set.<sup>4</sup>

The ground-state geometry of isolated mC was optimized using the B2PLYP double hybrid functional,<sup>5</sup> the def2-TZVPPD basis set and the conductor-like polarizable continuum solvation model of bulk water (C-PCM). Based on this geometry we simulated the vibrational frequencies for the electronic ground states applying the same approach, since it

was demonstrated that the B2PLYP functional accurately reproduces vibrational properties for medium-sized heteroaromatic molecules.<sup>6</sup> The vibrational frequencies in the S<sub>1</sub> and T<sub>1</sub> electronically excited states, were simulated numerically at the CC2/cc-pVTZ level of theory. Since the nature of the  $^1n\pi_{CT}^*$  state can be reproduced only with explicit water molecules, the calculations of excited-state vibrational frequencies were performed for the mC-(H<sub>2</sub>O)<sub>2</sub> cluster. All mobile protons (OH and NH) in the frequency calculations were exchanged to deuterium to better correlate with the reference time-resolved IR experimental measurements performed in D<sub>2</sub>O.

The excited-state UV-vis absorption (ESA) spectra were simulated in the S<sub>1</sub> and T<sub>1</sub> minima of the mC-(H<sub>2</sub>O)<sub>2</sub> cluster. Even though, these simulations do not yield a time-resolved transient absorption UV spectrum, they serve as a good tool to interpret such experiments by showing the characteristic absorption bands for the investigated excited-states. To simulate the ESA spectra we employed the nuclear ensemble method of Crespo-Otero and Barbatti,<sup>7</sup> and calculated oscillator strengths between the S<sub>1</sub> (or T<sub>1</sub>) and nine additional excited states within the given multiplicity. In each of the cases we generated 500 geometries using the Wigner distribution for all vibrational normal modes calculated in the S<sub>1</sub> and T<sub>1</sub> states respectively. The excitation energies and oscillator strengths were calculated at the CC2/cc-pVTZ level of theory and were validated against calculations performed using the EOM-CCSD/TZVP approach for the S<sub>1</sub> minimum-energy geometries (see below).<sup>3,8</sup>

The potential-energy profile for the electron-driven proton transfer (EDPT) process was calculated using the CC2/cc-pVTZ approach.<sup>2,3</sup> The geometries in the initial part of the profile were obtained from a relaxed scan along the C2=O...H-OH distance starting in the S<sub>1</sub> minimum. The further part of the profile was obtained by linear interpolation in internal coordinates (LIIC) between the last point of the relaxed scan and the EDPT conical intersection optimized at the MR-CISD level of theory.

The spin-orbit coupling matrix elements (SOCMEs) between the S<sub>1</sub> and T<sub>1</sub> states were calculated using the CASPT2/SA-CASSCF(6,5) approach and the cc-pVTZ-DK

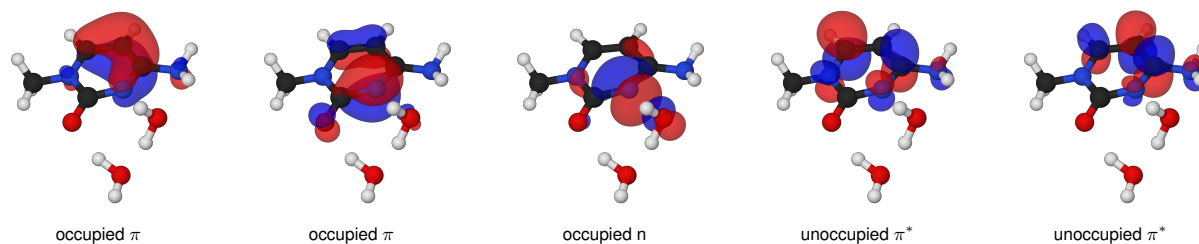


**Fig. S2** Molecular orbitals included in the active space in the CASPT2/SA3-CASSCF(6,5)/cc-pVTZ-DK calculations. The geometry presented above corresponds to the  $S_1$  minimum of the mC-(H<sub>2</sub>O)<sub>2</sub> cluster.

basis set. The scalar relativistic effects were estimated by means of the 2nd order Douglas-Kroll-Hess Hamiltonian. The value of the spin-orbit coupling provided in the main manuscript corresponds to the square root of the sum of squares of the SOCMEs.

The active space used in all the CASPT2/SA3-CASSCF(6,5) consisted of 2 occupied  $\pi$ , 1 occupied  $n$  and 2 virtual  $\pi^*$  molecular orbitals, e.g. 6 electrons were correlated in 5 orbitals. The CASSCF calculation was averaged over 3 electronic states. The choice of the active space was based on the rules proposed by Veryazov, Malmqvist and Roos,<sup>9</sup> which indicate that only orbitals with natural orbital occupations between 0.02-1.98 should be considered in CASSCF calculations.<sup>9</sup> This active space (6 electrons in 5 orbitals) was sufficient to correctly describe the  $S_1$  PE surface, especially in the vicinity of the  $S_1$  minimum and the EDPT  $S_1/S_0$  conical intersection. Majority of CASPT2/CASSCF calculations were performed with this setting. The cc-pVTZ-DK basis set was employed for single point calculations, while the 6-31G\* basis set was applied in the numerical optimization of the  $S_1$  minimum. The active space applied in the optimization of conical intersection at the MR-CISD level comprised of 4 electrons correlated in 3 orbitals (1 occupied, 1 occupied  $\pi$ , 1 occupied  $n$  and 1 virtual  $\pi^*$  molecular orbital). The CASSCF and CASVB calculations were performed for protonated mC in order to establish the importance of different resonance structures in this intermediate. The active space in these calculations consisted of 3 occupied  $\pi$  and 3 virtual  $\pi^*$  orbitals, thus correlating 6 electrons in 6 orbitals, and the 6-31G\*\* basis set was used.

All the CC2 and MP2 electronic structure calculations were performed with the TURBOMOLE 7.0 program,<sup>10</sup> while B2PLYP calculations were performed using the GAUSSIAN 09 package.<sup>11</sup> The CASPT2/CASSCF and CASVB calculations were carried out employing the MOLCAS 8.0 program,<sup>12</sup> while the MR-CISD calculations were performed using the COLUMBUS 7.0 package.<sup>13</sup> The simulations of the

excited-state UV-vis absorption spectra were performed using the Newton-X 1.4 package and an in-house script for handling the TURBOMOLE 7.0 and Newton-X 1.4 outputs in order to take into account the transitions between excited states.<sup>14</sup> The EOM-CCSD calculation was conducted with the Molpro 2012 package.<sup>15</sup> The CASPT2(C-PCM) optimization of the  $S_1$  minimum of the cytosine-(H<sub>2</sub>O)<sub>2</sub> was performed using the open-source external optimizer xopt, involving numerical gradients, approximate normal coordinates and a rational function approach for the stepsize.<sup>16,17</sup>

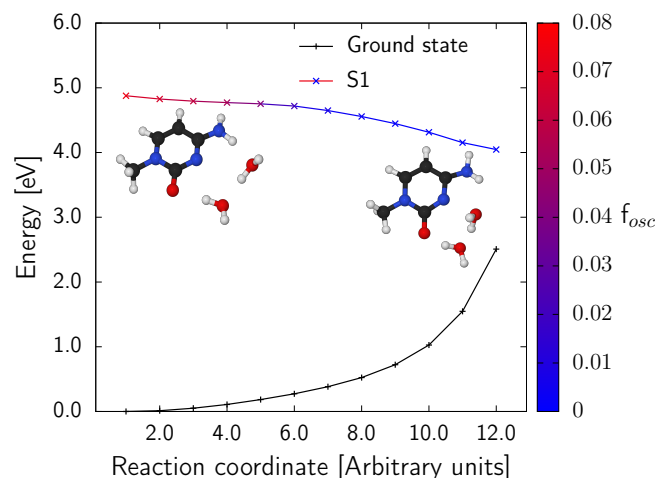


**Fig. S3** Potential energy profile for the plausible pathway from the Franck-Condon region to the  $S_1(n\pi^*_{CT})$  minimum. The oscillator strength corresponding to the  $S_0-S_1$  transition is marked with colors on the  $S_1$  dataset. The red color visible near the Franck-Condon region, corresponds to oscillator strengths close to 0.08 and the  $\pi\pi^*$  excitation. The blue color corresponds to very low oscillator strengths (near 0.0001) and the  $n_N\pi^*$  excitation. Therefore, the excitation character is changed along the PE profile from  $\pi\pi^*$  to  $n_N\pi^*$ .

## Molecular mechanism of the $n\pi_{CT}^*$ state population.

The plausible reaction path from the Franck-Condon region to the  $S_1(n\pi_{CT}^*)$  minimum is presented in Fig. S3. In this particular example, we assumed that the microsolvated mC chromophore is excited to the lowest lying bright  $\pi\pi^*$  ( $S_1$ ) state. The corresponding excitation energy of 254 nm, suggests that this state should be primarily populated in pump probe experiments which employ 267 nm as the pump wavelength.<sup>18</sup> Our calculations suggest that the pathway towards the  $S_1(n\pi_{CT}^*)$  minimum is barrierless. Along this path the contribution of the  $\pi\pi^*$  excited configuration is diminished in favor of the  $n_N\pi^*$  configuration. This observation is supported by the oscillator strength of the  $S_0$ - $S_1$  transition, which systematically decreases along the reaction coordinate. Therefore our predictions are in good agreement with the induced fluorescence measurements which almost entirely vanishes during the initial few picoseconds of the excited state dynamics of aquated cytidines.<sup>19</sup>

## Geometries of cytosine-( $H_2O$ )<sub>2</sub> and cytidine-( $H_2O$ )<sub>2</sub> clusters

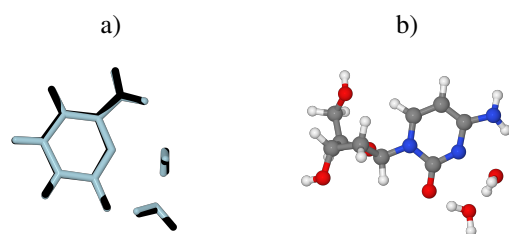


**Fig. S4**  $S_1(n\pi_{CT}^*)$  minima of cytosine-( $H_2O$ )<sub>2</sub> and cytidine-( $H_2O$ )<sub>2</sub> clusters: a) comparison of the cytosine-( $H_2O$ )<sub>2</sub> geometries optimized using the CASPT2/CASSCF(6,5)/6-31G\* (black) and CC2/cc-pVTZ (light blue) methods; b) geometry of the cytidine-( $H_2O$ )<sub>2</sub> cluster optimized using the CC2/cc-pVTZ method.

To test whether the CC2 method is capable of correctly predicting the geometry of the  $n\pi_{CT}^*$  state we performed additional optimization of this minimum using the CASPT2/SA-2-CASSCF(6,5)/6-31G\* approach. The CC2 (light blue) and CASPT2 (black) geometries are overlaid and shown in Fig. S4 a and reveal very good qualitative agreement, with minor quantitative difference. For instance, the  $H_2O \cdots N3$  distance amounts 2.09 and 2.19 Å at the CC2 and CASPT2 levels respectively. These results additionally validate the prediction of this distinctive geometry in our simulations.

Since large part of the photochemical processes addressed in this article were observed for cytidines (both ribo and de-

oxyribonucleosides and their anomers), we additionally optimized the corresponding minimum on the  $^1n\pi_{CT}^*$  hypersurface for deoxyribocytidine (see Fig. S4 b). This geometry exhibits all the qualitative features of the corresponding  $S_1$  minimum found for N1-methylcytosine (mC). Therefore, we anticipate that our observations for mC, are also valid for the various cytosine nucleosides.

## Single point benchmark CASPT2/SA-CASSCF calculations for the mC-( $H_2O$ )<sub>2</sub> cluster

To validate the CC2 calculations for the three most important stationary points on the  $S_1$  hypersurface we performed additional calculations at the CASPT2/SA3-CASSCF(6,5)/cc-pVTZ-DK level. The corresponding CASPT2 and CC2 energies are generally consistent and presented in Table. At the EDPT conical intersection geometry the CC2 calculations yielded negative excitation energy of the  $S_1$  state, and the CC2 method is no longer capable of correctly describing the electronic wave function in the region. Therefore, we performed the conical intersection optimization at the MR-CISD level and the insignificant energy gap of -0.16 eV (the closed shell configuration becomes dominant in the  $S_1$  stat) obtained at the CASPT2/cc-pVTZ-DK level validates the EDPT-CI geometry. Some discrepancy between the CASPT2 and CC2 methods is also evident for the adiabatic  $S_1$ - $S_0$  energy gap, however, the difference between these values is not dramatic and we conclude that the CC2 method is capable of providing a reliable qualitative description of the studied processes.

**Table 1** Relative energies [eV] at the most important stationary points obtained using the CC2/cc-pVTZ and CASPT2/cc-pVTZ-DK methods.

Description	CC2/[eV]	CASPT2/[eV]
$\Delta E_{S_1-S_0}$ Franck-Condon region	4.88	4.72
$\Delta E_{S_1-S_0}$ $S_1$ minimum	1.54	1.57
$\Delta E_{S_1-S_0}$ adiabatic	4.05	4.65
$\Delta E_{S_1-S_0}$ EDPT-CI geometry	-0.30	-0.16

Figure S5 presents the CASPT2 and CC2 energies computed along the PE profile corresponding to the electron driven proton transfer process (EDPT). The CASPT2 and CC2 methods yield qualitatively consistent results for this particular process, and thus, the usage of the CC2 method for the majority of the electronic structure calculations presented in this work is well justified. It is worth noting that the CASPT2 calculations suggest a higher barrier ( $\sim 0.27$  eV) for the EDPT process than the CC2 approach. This effect may originate from the fact that the optimized geometries were relaxed at the CC2

level. In addition, this barrier is most likely overestimated due to the interpolation procedure. Nevertheless, the barrier estimated at the CASPT2 level is still rather low and can be easily overcome considering the excess vibrational energy of the hot, UV-excited chromophore.

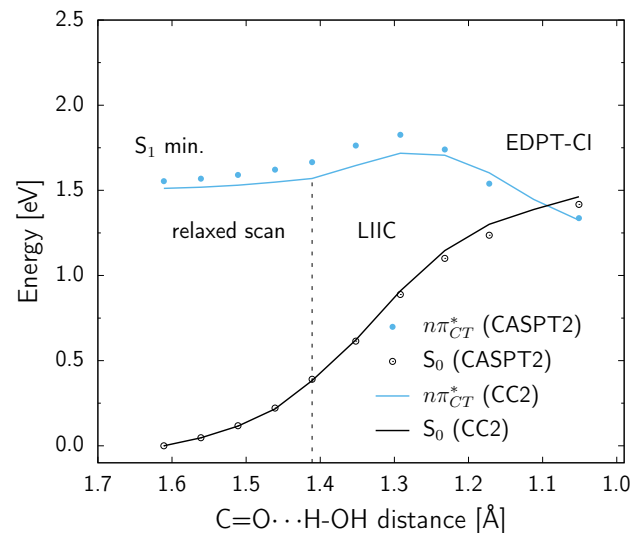


**Fig. S5** Potential energy profile presenting the electron-driven proton transfer mechanism which may occur on the  $^1n\pi_{CT}^*$  hypersurface. All energies and the geometries corresponding to the relaxed scan from the  $S_1$  minimum along the C=O...H-OH distance were obtained at the CC2/cc-pVTZ level. LIIC - linear interpolation in internal coordinates between the last geometry of the relaxed scan and the conical intersection geometry obtained using the MR-CISD(4,3)/6-31G\* method. The points present the CASPT2/SA3-CASSCF(6,5)/cc-pVTZ-DK energies calculated along the PE profile.

### Geometry of the methylcytosine-(H<sub>2</sub>O)<sub>5</sub> cluster in the S<sub>1</sub> state

In order to show that the  $n\pi_{CT}^*$  state is the lowest-lying singlet state in larger mC-water clusters, we additionally performed  $S_1$  geometry optimization of a mC-(H<sub>2</sub>O)<sub>5</sub> cluster at the CC2/aug-cc-pVDZ level. The corresponding  $S_1$  minimum geometry exhibits the characteristic features found for the smaller clusters containing just two water molecules, including the H<sub>2</sub>O...N3 interaction (2.07 Å). Interestingly, during the optimization procedure, one of the water molecules initially placed at the amino group moved below the aromatic ring. This is associated with the formation of an interaction between the H<sub>2</sub>O proton and the negatively charged aromatic ring. We anticipate that such arrangement of water molecule above and below the aromatic ring in bulk water, could additionally stabilize the charge-transfer character of the  $^1n\pi^*$

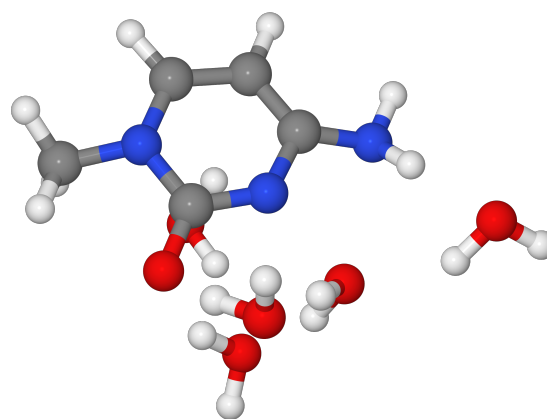


**Fig. S6** The  $S_1$  minimum energy geometry of the mC-(H<sub>2</sub>O)<sub>5</sub> cluster optimized at the CC2/aug-cc-pVDZ level of theory.

state. This observation along with the comparison of simulated and experimental spectra suggest that the conclusions drawn here for the mC-water clusters of limited size are most likely valid for bulk environments and should provide a qualitatively correct picture of the studied processes.

### Simulations of vibrational frequencies in the T<sub>1</sub> minimum and comparison to the experimental TR-IR spectrum

The harmonic vibrational frequencies of the mC-(H<sub>2</sub>O)<sub>2</sub> cluster simulated for the T<sub>1</sub>( $\pi\pi^*$ ) minimum-energy geometry using the same CC2 approach are presented in Fig. 3 in the main article. Interestingly the C=O stretching band is centred at 1560 cm<sup>-1</sup> similarly as in the case of the  $S_1$  state. However, our frequency simulations for the T<sub>1</sub> indicate that there are only two vibrations with intensities high enough to be visible in the TR-IR absorption spectra, and not three as concluded from the analysis of the experimental spectrum (the other simulated vibration corresponds to C4=C5 stretching and can be located at 1630 cm<sup>-1</sup>). Furthermore, the simulations of excited-state UV-vis absorption (ESA) spectra presented in the main article (Fig. 4), eventually confirm that the dark state cannot be assigned as the lowest-lying triplet state, after the comparison to experimental broadband TA-UV measurements performed by Ma et al.<sup>19</sup>

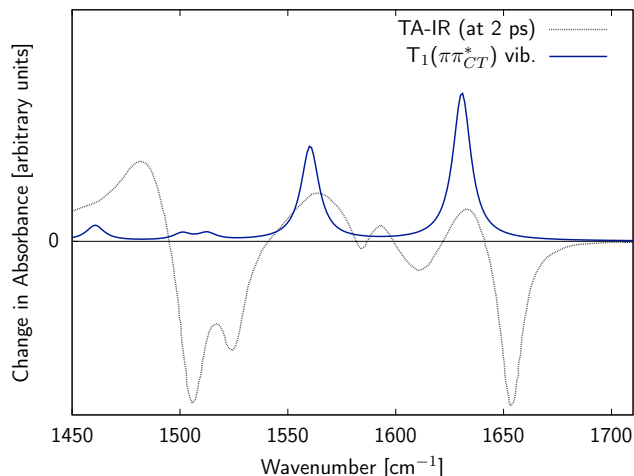


**Fig. S7** Harmonic vibrational frequencies (in the range 1450 to 1750  $\text{cm}^{-1}$  calculated in the  $T_1$  minimum of the  $mC-(H_2O)_2$  cluster. The experimental TR-IR spectrum from ref. 20 is overlaid with the theoretical data.

**Table 2** Vertical excitation energies calculated in the  $S_1(n\pi_{CT}^*)$  minimum for the transitions from the  $S_1$  state to higher excited singlet states

Transition	$E_{exc}$ [eV]	$f_{osc}$ ( $S_1 \rightarrow S_{n+1}$ )	$\lambda$ [nm]
CC2/cc-pVTZ			
$S_1 \rightarrow S_2$	2.07	$1.23 \cdot 10^{-2}$	599.0
$S_1 \rightarrow S_3$	2.47	$5.99 \cdot 10^{-2}$	502.0
$S_1 \rightarrow S_4$	3.01	$9.87 \cdot 10^{-6}$	411.9
$S_1 \rightarrow S_5$	3.17	$3.34 \cdot 10^{-2}$	391.1
$S_1 \rightarrow S_6$	3.25	$7.37 \cdot 10^{-4}$	381.5
$S_1 \rightarrow S_7$	3.50	$4.03 \cdot 10^{-3}$	354.2
$S_1 \rightarrow S_8$	3.90	$2.14 \cdot 10^{-3}$	317.9
$S_1 \rightarrow S_9$	4.37	$1.50 \cdot 10^{-3}$	283.7
EOM-CCSD/TZVP			
$S_1 \rightarrow S_2$	2.04	$1.46 \cdot 10^{-2}$	607.8
$S_1 \rightarrow S_3$	2.26	$1.42 \cdot 10^{-4}$	548.6
$S_1 \rightarrow S_4$	2.93	$4.21 \cdot 10^{-4}$	423.2
$S_1 \rightarrow S_5$	3.26	$3.55 \cdot 10^{-3}$	380.3
$S_1 \rightarrow S_6$	3.63	$4.08 \cdot 10^{-4}$	341.6
$S_1 \rightarrow S_7$	3.98	$2.12 \cdot 10^{-3}$	311.5
$S_1 \rightarrow S_8$	4.01	$2.87 \cdot 10^{-4}$	309.2
$S_1 \rightarrow S_9$	4.45	$1.33 \cdot 10^{-3}$	278.6

### Benchmark calculations for the excitation energies calculated from the $S_1$ minimum.

The vertical excitation energies calculated in the  $S_1(n\pi_{CT}^*)$  minimum are presented in Table 2. The two sets of results were computed using the CC2/cc-pVTZ and EOM-

CCSD/TZVP methods. The CC2/cc-pVTZ method was used to simulate the excited state absorption spectrum presented in Fig. 4 in the main article. The CC2 results are generally consistent benchmark calculations performed using the EOM-CCSD/TZVP approach and the energy deviations for most of the listed transitions do not exceed 0.2 eV. However, the energies of two transitions ( $S_1 \rightarrow S_6$  and  $S_1 \rightarrow S_7$ ) might be underestimated by the CC2 method by 0.4 to 0.5 eV. Although these differences are already considerable and some ESA spectral features might be unnaturally redshifted (e.g. from  $\sim 310$  nm to 350 nm) by the CC2 method, the agreement between these approaches is decent and the ESA spectrum should be qualitatively reproduced. Indeed, the simulated excited-state absorption (ESA) spectrum is qualitatively consistent with the TA-UV measurements,<sup>19</sup> and the onset of the excited-state absorption band (at 360 nm) is slightly redshifted with respect to the experimental value of  $\sim 330$  nm.<sup>19</sup> We stress that the ESA simulations from the  $S_1$  minimum were quite challenging and we already saw some discrepancies between the CC2/cc-pVDZ and CC2/cc-pVTZ approaches. Therefore we decided to perform ESA spectra simulations using the larger cc-pVTZ basis set and additionally benchmark the simulations from the  $S_1$  minimum against the EOM-CCSD/TZVP values. In comparison, the cc-pVDZ and cc-pVTZ basis sets gave very similar results for the vertical excitation energies simulated from the  $T_1$  minimum, however, to keep consistency with the former results we also employed the CC2/cc-pVTZ approach for the  $T_1$  ESA spectrum.

## Analysis of the CASSCF and CASVB calculations of protonated mC

The analysis of the CASSCF wave function in terms of the spin-coupled valence bond structures using the CASVB approach provides additional information about the importance of the resonance structures of protonated mC (ground-state intermediate formed in the photoinduced EDPT process), shown in Fig. 5 in the main article. According to these calculations, the resonance structure with the dominant weight is characterized by C5=C6 and C2=N3 double bonds and the positive charge residing on the C4 atom. Consequently, the nucleophilic addition of the hydroxide anion in the C4 position is a highly plausible process and it explains the C to U conversion reaction which still requires one further step, e.g. deamination. Even though the wave function analysis does not indicate high contribution of the two remaining resonance structures shown in Fig. 5 in the main article, the population analysis suggests that the C2, C4 and C6 carbon atoms are positively charged (+0.99, +0.65 and +0.21 respectively) and prone to additions of nucleophiles.

## References

- 1 F. Weigend and M. Häser, *Theoretical Chemistry Accounts*, 1997, **97**, 331–340.
- 2 C. Hättig, *Adv. Quantum Chem.*, 2005, **50**, 37–60.
- 3 C. Hättig and F. Weigend, *J. Chem. Phys.*, **113**, 5154–5161.
- 4 J. Finley, P.-A. Malmqvist, B. O. Roos and L. Serrano-Andres, *Chem. Phys. Lett.*, **288**, 299–306.
- 5 S. Grimme, *J. Chem. Phys.*, **124**, 034108.
- 6 M. Biczysko, P. Panek, G. Scalmani, J. Bloino and V. Barone, *J. Chem. Theory Comput.*, **6**, 2115–2125.
- 7 R. Crespo-Otero and M. Barbatti, *Theor. Chem. Acc.*, 2012, **131**, 1–14.
- 8 C. Hättig and A. Köhn, *J. Chem. Phys.*, **117**, 6939–6951.
- 9 V. Veryazov, P. Å. Malmqvist and B. O. Roos, *Int. J. Quantum Chem.*, 2011, **111**, 3329–3338.
- 10 R. Ahlrichs, M. Bär, M. Häser, H. Horn and C. Kölmel, *Chemical Physics Letters*, 1989, **162**, 165–169.
- 11 M. J. Frisch, G. W. Trucks, H. B. Schlegel, G. E. Scuseria, M. A. Robb, J. R. Cheeseman, G. Scalmani, V. Barone, B. Mennucci, G. A. Petersson, H. Nakatsuji, M. Caricato, X. Li, H. P. Hratchian, A. F. Izmaylov, J. Bloino, G. Zheng, J. L. Sonnenberg, M. Hada, M. Ehara, K. Toyota, R. Fukuda, J. Hasegawa, M. Ishida, T. Nakajima, Y. Honda, O. Kitao, H. Nakai, T. Vreven, J. Montgomery, J. E. Peralta, F. Ogliaro, M. Bearpark, J. J. Heyd, E. Brothers, K. N. Kudin, V. N. Staroverov, R. Kobayashi, J. Normand, K. Raghavachari, A. Rendell, J. C. Burant, S. S. Iyengar, J. Tomasi, M. Cossi, N. Rega, J. M. Millam, M. Klene, J. E. Knox, J. B. Cross, V. Bakken, C. Adamo, J. Jaramillo, R. Gomperts, R. E. Stratmann, O. Yazyev, A. J. Austin, R. Cammi, C. Pomelli, J. W. Ochterski, R. L. Martin, K. Morokuma, V. G. Zakrzewski, G. A. Voth, P. Salvador, J. J. Dannenberg, S. Dapprich, A. D. Daniels, O. Farkas, J. B. Foresman, J. V. Ortiz, J. Cioslowski and D. J. Fox, *Gaussian 09, revision C.01*, 2009, Gaussian Inc. Wallingford CT.
- 12 F. Aquilante, J. Autschbach, R. K. Carlson, L. F. Chibotaru, M. G. Delcey, L. De Vico, I. Fdez. Galván, N. Ferré, L. M. Frutos, L. Gagliardi, M. Garavelli, A. Giussani, C. E. Hoyer, G. Li Manni, H. Lischka, D. Ma, P. Å. Malmqvist, T. Müller, A. Nenov, M. Olivucci, T. B. Pedersen, D. Peng, F. Plasser, B. Pritchard, M. Reiher, I. Rivalta, I. Schapiro, J. Segarra-Martí, M. Stenrup, D. G. Truhlar, L. Ungur, A. Valentini, S. Vancoillie, V. Veryazov, V. P. Vysotskiy, O. Weingart, F. Zapata and R. Lindh, *Journal of Computational Chemistry*, 2016, **37**, 506–541.
- 13 H. Lischka, R. Shepard, I. Shavitt, R. M. Pitzer, M. Dallos, T. Müller, P. G. Szalay, F. B. Brown, R. Ahlrichs, H. J. Böhm, A. Chang, D. C. Comeau, R. Gdanitz, H. Dachsels, C. Ehrhardt, M. Ernzerhof, P. Höchtl, S. Irle, G. Kedziora, T. Kovar, V. Parasuk, M. J. M. Pepper, P. Scharf, H. Schiffer, M. Schindler, M. Schüler, M. Seth, E. A. Stahlberg, J.-G. Zhao, S. Yabushita, Z. Zhang, M. Barbatti, S. Matsika, M. Schuurmann, D. R. Yarkony, S. R. Brozell, E. V. Beck, J.-P. Blaudeau, M. Ruckebauer, B. Sellner, F. Plasser and J. J. Szymczak, *Columbus, Release 7.0 2012, an Ab Initio Electronic Structure Program*, 2012.
- 14 M. Barbatti, M. Ruckebauer, F. Plasser, J. Pittner, G. Granucci, M. Persico and H. Lischka, *Wiley Interdiscip. Rev.: Comput. Mol. Sci.*, 2014, **4**, 26–33.
- 15 H.-J. Werner, P. J. Knowles, G. Knizia, F. R. Manby and M. Schütz, *Wiley Interdiscip. Rev.: Comput. Mol. Sci.*, 2012, **2**, 242–253.
- 16 H. Kruse, <https://github.com/hokru/xopt>; local development version., 2016, Institute of Biophysics, Brno.
- 17 F. Eckert, P. Pulay and H.-J. Werner, *J. Comput. Chem.*, 1997, **18**, 1473–1483.
- 18 P. M. Hare, C. E. Crespo-Hernández and B. Kohler, *Proc. Natl. Acad. Sci.*, 2007, **104**, 435–440.
- 19 C. Ma, C. C.-W. Cheng, C. T.-L. Chan, R. C.-T. Chan and W.-M. Kwok, *Phys. Chem. Chem. Phys.*, 2015, **17**, 19045–19057.
- 20 P. M. Keane, M. Wojdyla, G. W. Doorley, G. W. Watson, I. P. Clark, G. M. Greetham, A. W. Parker, M. Towrie, J. M. Kelly and S. J. Quinn, *J. Am. Chem. Soc.*, 2011, **133**, 4212–4215.

---

## Cartesian coordinates of the crucial stationary points considered in the article

**S<sub>0</sub> and T<sub>1</sub> minimum energy geometries of the mC-(H<sub>2</sub>O)<sub>2</sub> cluster optimized at the MP2 and CC2 levels respectively.**

Ground-state geometry

N	2.956599	0.084420	0.119875
C	2.014515	0.008097	-0.923377
N	0.700337	0.001625	-0.600988
C	0.307417	0.030454	0.660456
C	1.237049	0.097671	1.744490
C	2.553944	0.123663	1.412260
O	2.425227	-0.058933	-2.086807
N	-1.018459	0.013188	0.880521
C	4.361562	0.088012	-0.253562
O	-0.095423	-0.871685	-3.320706
H	0.927126	0.129835	2.776339
H	3.339359	0.174418	2.153254
H	-1.370917	-0.108105	1.810445
H	-1.617614	-0.141955	0.066481
H	4.561453	0.921022	-0.921731
H	4.960502	0.178563	0.647931
H	4.609062	-0.831927	-0.776946
H	0.728199	-0.552411	-2.910680
H	0.032515	-0.740667	-4.261506
O	-2.314787	-0.378472	-1.654144
H	-1.525121	-0.580308	-2.194703
H	-2.614336	0.457665	-2.017599

T1 minimum-energy geometry

N	2.940522	0.304879	0.044308
C	1.994946	0.118338	-0.911083
N	0.689225	0.471187	-0.532741
C	0.293156	-0.100732	0.717584
C	1.184749	0.131288	1.729307
C	2.510788	0.524178	1.364305
O	2.199170	-0.311408	-2.063425
N	-0.913100	-0.725734	0.705348
C	4.327405	-0.037594	-0.226959
O	-0.260492	-0.970692	-3.288735
H	0.913577	0.034474	2.773107
H	3.269479	0.823110	2.069155
H	-1.308563	-0.983968	1.594319
H	-1.545828	-0.466417	-0.057965
H	4.468685	-0.053961	-1.303975
H	4.971580	0.717637	0.219579
H	4.572500	-1.015634	0.187385
H	0.610253	-0.739037	-2.913314
H	-0.210715	-0.678938	-4.203214
O	-2.184921	0.186218	-1.672878
H	-1.557390	-0.251947	-2.286407
H	-1.806815	1.068924	-1.594402

---

**S<sub>1</sub> minimum and the S<sub>1</sub>/S<sub>0</sub> conical intersection located along the EDPT reaction path for the mC-(H<sub>2</sub>O)<sub>2</sub> cluster (optimized using the CC2 and MR-CISD methods).**

S1 minimum				EDPT Conical intersection			
N	2.694480	0.153117	-0.022367	N	2.697016	0.220398	-0.005726
C	1.660475	0.172437	-0.948850	C	1.652202	0.206836	-0.835993
N	0.427370	0.128379	-0.412774	N	0.436852	0.138175	-0.428288
C	0.094472	-0.149685	0.927807	C	0.129353	-0.127859	0.880473
C	1.119925	-0.118539	1.825013	C	1.133616	-0.200769	1.794894
C	2.436601	0.095391	1.364030	C	2.454005	0.018085	1.367718
O	1.880737	0.257401	-2.184115	O	1.915184	0.299239	-2.126132
N	-1.229797	-0.513886	1.131015	N	-1.210295	-0.339559	1.098361
C	4.069169	0.166608	-0.477132	C	4.046311	0.380415	-0.497458
O	0.042892	-1.255131	-3.286052	O	0.088844	-1.292732	-3.181412
H	0.940608	-0.286737	2.879302	H	0.929132	-0.402496	2.831340
H	3.297562	0.183914	2.006631	H	3.308759	0.055766	2.007996
H	-1.548348	-0.335079	2.072340	H	-1.565244	-0.141013	2.011673
H	-1.840405	-0.114457	0.429823	H	-1.785548	-0.030249	0.334954
H	4.065934	0.244507	-1.559509	H	4.008968	0.700814	-1.526639
H	4.593450	1.022948	-0.048196	H	4.550747	1.135399	0.094755
H	4.578128	-0.749465	-0.171135	H	4.588579	-0.557515	-0.434117
H	0.858825	-0.758306	-3.011375	H	1.242186	-0.236843	-2.617486
H	-0.029469	-1.123525	-4.236336	H	-0.060549	-1.223768	-4.120253
O	-1.241164	0.269803	-1.665402	O	-1.240572	0.303116	-1.687096
H	-0.845603	-0.375566	-2.346377	H	-0.610429	-0.773449	-2.721626
H	-0.867632	1.130040	-1.917041	H	-0.903191	1.148010	-1.996306